

L. KERNAZHITSKY,¹ V. SHYMANOVSKA,¹ T. GAVRILKO,¹ V. NAUMOV,¹
L. FEDORENKO,² V. KSHNYAKIN,³ J. BARAN⁴

¹Institute of Physics, Nat. Acad. of Sci. of Ukraine

(46, Prosp. Nauky, Kyiv 03028, Ukraine; e-mail: kern@iop.kiev.ua)

²Lashkaryov Institute of Semiconductor Physics, Nat. Acad. of Sci. of Ukraine,

(45, Prosp. Nauky, Kyiv 03028, Ukraine)

³Sumy State University

(2, Rymtsky-Korsakov Str., Sumy 40007, Ukraine)

⁴Institute of Low Temperature and Structure Research, Polish Academy of Sciences

(2, Okolna Str., 50-950 Wroclaw, Poland)

PACS 61.46.+w, 61.72.Ji,
71.35.-y, 33.50.Dq

LASER-EXCITED EXCITONIC LUMINESCENCE OF NANOCRYSTALLINE TiO₂ POWDER

Titanium dioxide (TiO₂) nanocrystalline powders were prepared by the thermal hydrolysis method in the form of pure anatase or rutile and were investigated by X-ray diffraction, X-ray fluorescence, FT-Raman spectroscopy, optical absorption, and photoluminescence (PL) methods. PL spectra were studied under the intense UV laser excitation at 337.1 nm (3.68 eV) at room temperature. Some interesting features in the PL spectra including the well-resolved peaks of excitonic and band-band transitions in TiO₂ were observed for the first time. It is shown that PL bands with peaks at 2.71–2.81 eV and its phonon replicas in anatase and rutile TiO₂ arise from the excitonic $e^- - h^+$ recombination via oxygen vacancies. The excitonic peak at 2.91 eV is attributed to the recombination of self-trapped excitons in anatase or free excitons in rutile TiO₂. The PL peaks within 3.0–3.3 eV in anatase TiO₂ are ascribed to indirect allowed transitions due to the band-band $e^- - h^+$ recombination. The peaks at 3.03 and 3.26 eV are attributed to the free exciton emission near the fundamental band edge of rutile and anatase TiO₂, respectively.

Keywords: titanium dioxide, anatase, rutile, UV-vis spectroscopy, photoluminescence.

1. Introduction

Nanostructured TiO₂ is a well-known wide-band semiconductor material that is widely used in photovoltaics, photocatalysis, photosensors, etc. [1–3]. Physical properties of TiO₂ are essentially dependent on synthesis methods responsible for its chemical purity and crystal form (anatase or rutile), as well as on particle features such as crystallinity, shape, specific surface area, and surface chemistry [2]. They also depend on the defect states in the crystal lattice of TiO₂ which affect the excitation and relaxation of photoexcited carriers [3]. In TiO₂ studies, the laser-excited photoluminescence (PL) technique is often used to investigate the structure and properties of the active sites on the surface, the efficiency of the charge carrier trapping, migration, and transfer

in order to understand the behavior of electron-hole pairs in TiO₂, because of its high sensitivity and non-destructive character [4, 5]. However, as reported in the literature, it is difficult to observe any PL emission at room temperature for the bulk TiO₂, even in the single crystal state, due to its indirect transition nature [6].

The low-temperature PL for anatase TiO₂ crystals with a broad emission band at 2.3 eV was observed by Tang *et al.* [7], and it was attributed to the recombination of self-trapped excitons (STE) [8]. De Haart and Blasse [9] ascribed a sharp peak observed at 3.01 eV in low-temperature PL spectra of rutile TiO₂ crystals to the free exciton emission, and a broad band at 2.55 eV to the bound exciton due to the trapping of free excitons by Ti groups near the defect states. Amtout and Leonelli [10] suggested that the photoresponse near the band gap in the range at 2.7–3.0 eV originated from the phonon replicas of the 1s exciton.

© L. KERNAZHITSKY, V. SHYMANOVSKA,
T. GAVRILKO, V. NAUMOV, L. FEDORENKO,
V. KSHNYAKIN, J. BARAN, 2014

The temperature dependences of PL spectra for polydisperse anatase and rutile TiO₂ were studied in the range 5–180 K by Melnik *et al.* [11]. It was shown that polydisperse anatase has two PL bands at 3.1 and 2.3 eV, whereas polydisperse rutile has one PL band at 3.0 eV. With increasing temperature from 5 K to 140 K, the intensity of both PL bands decreases.

The room-temperature PL for nanostructured TiO₂ was studied in several works. Serpone *et al.* [12] explored the PL of anatase TiO₂ colloidal particles with different sizes and found that PL occurs from the shallow trap levels located between 0.41 and 0.64 eV below the conduction band (CB). Saraf *et al.* [13] found that the narrow PL emission of anatase TiO₂ powder originated from the STE on TiO₆ octahedra.

In this work, we studied the PL of single-phase nanocrystalline anatase (*A*) and rutile (*R*) TiO₂ powders at room temperature. The high-purity *R* and *A* TiO₂ samples were synthesized by the thermal hydrolysis method and characterized by X-ray diffraction, FT-Raman, UV-vis optical absorption, and PL spectroscopy. The data obtained for the studied TiO₂ samples by different techniques were compared, and the relationships between the structural and PL properties for *A* and *R* modifications were analyzed.

2. Experimental

2.1. Samples preparation

For the research, we prepared high-purity polydisperse nanocrystalline TiO₂ powders with *R* and *A* structures. The TiO₂ samples were synthesized by the thermal hydrolysis of TiCl₄ hydrochloric acid solutions at 100 °C in the presence of *R* or *A* colloidal titanium nuclei [14]. For instance, the TiCl₄ hydrochloric acid solution (100 g/l TiO₂) with 3.0 TiO₂/HCl relative molar concentration was added with 3 wt.% colloidal titanium nucleus of rutile, kept at 100 °C for 3 h, and cooled down to room temperature. The residual precipitate was filtered and calcined at 200 °C for 5 h. The obtained TiO₂ samples were thoroughly washed with bi-distilled water up to pH = 6.5 and thermally treated in air at 300 °C.

2.2. Experimental methods

The structural properties and phase composition of the synthesized TiO₂ samples were determined by X-ray diffractometry (XRD) using a DRON-2 diffrac-

tometer with Cu_{Kα} (λ = 1.5406 Å) and Co_{Kα} (λ = 1.7902 Å) radiation. The mean crystallite sizes of *A* and *R* TiO₂ were evaluated from the *A* (101) and *R* (110) diffraction peaks using the Debye-Scherrer formula

$$D = K\lambda/\beta \cos \theta, \quad (1)$$

where *D* is the mean crystallite size, *K* is the constant which is taken as 0.89, λ is the wavelength of the X-ray radiation, β is the reflection full width at half maximum (FWHM), and θ is the diffraction angle. The specific surface area of TiO₂ samples was measured by the Brunauer-Emmett-Teller (BET) method similar to [11].

FT-Raman spectra of TiO₂ samples were measured with a Bruker IFS-88 spectrometer (spectral range of 380–4000 cm⁻¹, 2 cm⁻¹ spectral resolution) equipped with an FRA-106/S attachment with a Nd:YAG laser (λ = 1.064 μm, 300 mW power) and an InGaAs detector using the backscattering geometry of measurements.

The UV-vis absorption and PL spectra of TiO₂ samples were measured by a portable multichannel optical spectrum analyzer Solar SL40-2 (3648-pixel CCD sensor TCD1304AP, diffraction grating 600 l/mm, spectral resolution ~0.3 nm). UV-vis absorption spectra were recorded in the spectral range of 220–750 nm using DDC-30 deuterium (λ_{1 max} = 245 nm, λ_{max} = 311 nm) and DKSH-1000 xenon (λ_{ex} = 472 nm) lamps as the light sources. The PL spectra of TiO₂ samples were excited by a pulsed N₂ laser (λ_{ex} = 337.1 nm, pulse energy 50 μJ, pulse duration 7 ns, repetition rate 50 Hz, beam aperture ~1 mm). The special optical interference filters were used to discriminate the laser light and the laser-excited luminescence. PL was measured in the backscattering configuration. The samples for UV-vis absorption studies were prepared using the KBr pellet technique with a TiO₂/KBr ratio of ~0.1 wt.%. All measurements were carried out at room temperature.

3. Results and Discussion

3.1. XRD analysis

According to XRD characterization (Table 1), the prepared *A* and *R* TiO₂ samples have a well crystallized pure-phase structure. The mean sizes of nanocrystallites in polydisperse TiO₂ powders, determined from XRD patterns under Cu_{Kα} irradiation,

Table 1. Characterization of prepared TiO₂ samples

Samples	Crystal structure	Calculation temperature, °C	Mean crystallite size (±3), nm	Stoichiometry (±0.01)	BET, m ² /g
A	Anatase	300 °C	13	1.98	137
R	Rutile	300 °C	21	1.99	15

Table 2. Raman active optical phonon modes of rutile and anatase TiO₂ samples

Rutile			Anatase		
Raman shift (cm ⁻¹)	Assignment	Published data (cm ⁻¹)	Raman shift (cm ⁻¹)	Assignment	Published data (cm ⁻¹)
144	B _{1g}	143 ^a , 144 ^b , 143 ^c	146	E _g	153 ^a , 147 ^b
235	–	245 ^a , 235 ^b	194	E _g	201 ^a , 198 ^b
445	E _g	443 ^a , 448 ^b , 447 ^c	395	B _{1g}	402 ^a , 400 ^b
610	A _{1g}	612 ^a , 612 ^b , 612 ^c	514	A _{1g} , B _{1g}	522 ^a , 515 ^b
826	B _{2g}	833 ^a , 827 ^b , 826 ^c	636	E _g	643 ^a , 640 ^b

^a[16], ^b[17], ^c[15].

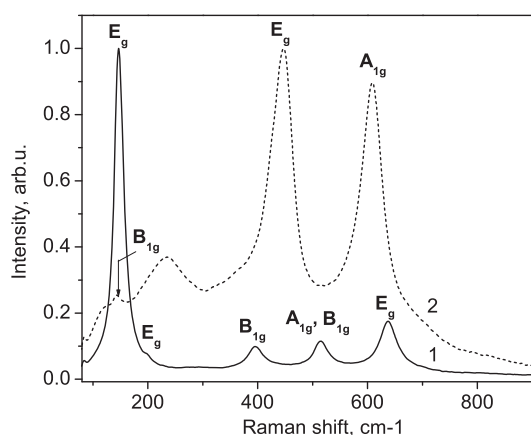


Fig. 1. Raman spectra of anatase A (1) and rutile (2) powders

appeared to be equal to 13 and 21 nm for A and R samples, respectively (see Table 1).

3.2. FT-Raman spectroscopy

The room-temperature FT-Raman spectra of the prepared A and R TiO₂ powders are typical of A and R crystalline phases (Fig. 1). In the Raman spectra of R TiO₂, three Raman-active optical phonon modes at 144, 445, and 610 cm⁻¹ are well observed. According to [15], these fundamental phonons are attributed to the B_{1g}, E_g, and A_{1g} modes, correspondingly. The low-intensity Raman mode with B_{2g} symmetry centered at 826 cm⁻¹ is poorly observed in our measure-

ments. A noticeable broad band at 235 cm⁻¹ observed in R TiO₂ does not coincide with any theoretical calculations for the fundamental modes allowed by symmetry in this phase. The nature of this Raman band is discussed in the literature [15–17], and it is suggested that it might be either second-order or disorder-induced scattering.

In the Raman spectra of A TiO₂, five Raman-active optical phonon modes are observed: 146 cm⁻¹ (E_g), 194 cm⁻¹ (E_g), 395 cm⁻¹ (B_{1g}), 514 cm⁻¹ (combination of A_{1g} and B_{1g} that cannot be resolved at room temperature [15]), and 636 cm⁻¹ (E_g). The frequencies of Raman-active modes, their assignment, and reference data on the powder [16, 17] and single crystal [15] for R and A TiO₂ are summarized in Table 2.

It is well established [18] that the position of the E_g Raman mode for A TiO₂ between 143 and 147 cm⁻¹ depends on the stoichiometric ratio O/Ti. For R TiO₂, the phonon mode E_g (446 cm⁻¹), attributed to in-plane bands of O–O bond [18], is also sensitive to the presence of oxygen vacancies in TiO₂. Based on the measured E_g peak position and its half-width (Fig. 1), the stoichiometry was determined for the studied A and R TiO₂ samples (Table 1).

3.3. UV-vis absorption spectroscopy

In the room-temperature UV absorption spectra, several peaks and features near the UV absorption

edge (2.8–3.4 eV) are observed both for *A* and *R* TiO₂ samples (Fig. 2) centered at 2.80, 2.85, 2.91, 2.92, and 2.93 eV (Fig. 2, inset). Some of these bands were previously observed by Ghosh *et al.* [19] under the thermal excitation of rutile single crystals. Khomenko *et al.* [20] have also observed weak absorption bands between 2.3 eV and 2.9 eV and assigned them to *d* – *d* transitions associated with Ti³⁺ localized states. It was suggested that the mentioned UV absorption peaks can be associated with the existence of defect levels inside the band gap. According to Daude *et al.* [21], the energy of the lowest phonon-assisted indirect allowed (IA) transition from the valence band (VB) to the conduction band (CB) is 2.91 eV. We suggest that, in our case, the UV absorption peaks at 2.91–2.93 eV can be assigned to the overlapping of the lowest-energy fundamental absorption and absorption by various defect states, e.g. Ti³⁺ localized states or electron transitions from different trap levels associated with oxygen vacancies.

One can see that *A* TiO₂ shows an exponential absorption edge at $h\nu > 3.0$ eV, which is much less steeper than that of *R* TiO₂. The differences in the UV-vis absorption spectra for *A* and *R* in this area originate from the different nature of excitons in these structures, namely, free excitons in *R* and self-trapped excitons in *A* TiO₂ [6]. Similar absorption spectra were observed at low temperatures for a single crystal TiO₂ [22] but, to the best of our knowledge, we observed the absorption spectrum for the first time for a nanocrystalline TiO₂ powder at room temperature.

As is seen in Fig. 2, the features at 3.05, 3.10, and 3.20 eV are characterized by changing the slope of the tangent to the absorption curve. According to Daude *et al.* [21], these features can be associated with the fundamental (or intrinsic) absorption of *R* or *A* TiO₂. Thus, the features at 2.91 and 3.05 eV can be assigned to indirect allowed (IA) transitions from the edge to the center of the Brillouin zone, namely, $X_{1a} \rightarrow \Gamma_{1b}$, and $X_{2b} \rightarrow \Gamma_{1b}$, respectively. The features at 3.10–3.20 eV and above 3.2 eV can be assigned to the $\Gamma_3 \rightarrow X_1$ IA transition and the onset of a direct allowed (DA) optical transition, respectively. Analogous observations of direct and indirect transitions in TiO₂ were also reported for single crystals by Vos and Krusemeyer [23] and for colloidal anatase particles by Serpone *et al.* [12].

3.4. PL spectroscopy

Figures 3 and 4 show the room-temperature PL spectra of the *R* and *A* TiO₂ powders. In the spectral range from 2.3 to 3.3 eV, a broad PL band is observed along with the presence of well-resolved narrow peaks. It is known that the PL intensity and the band structure depend on the excitation source power. With the use of ordinary commercial fluorimeters, a broad emission with a sharp peak at 2.91 eV [9, 12, 24–26] can be observed. The authors of [7, 11, 27, and 28] reported only a broad structureless emission in this range.

As was shown by Abazovic *et al.* [29], two intense peaks at 2.92 and 2.84 eV in TiO₂ PL were registered,

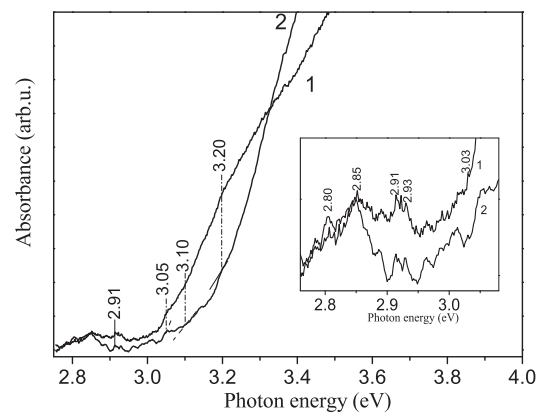


Fig. 2. UV-vis absorption spectra for rutile *R* (1) and anatase *A* (2) TiO₂. The dash lines show the tangent to the absorption curve. The inset displays the absorption spectra in 2.7–3.08 eV range

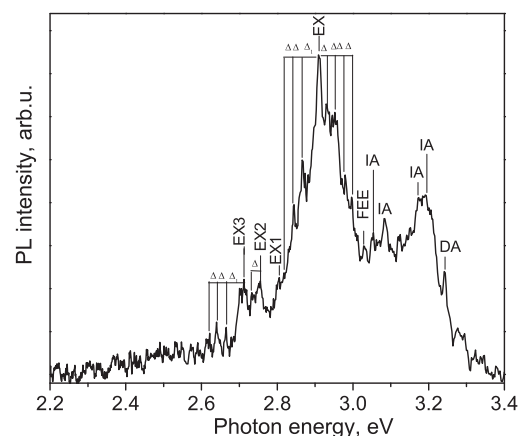


Fig. 3. PL spectrum of rutile sample

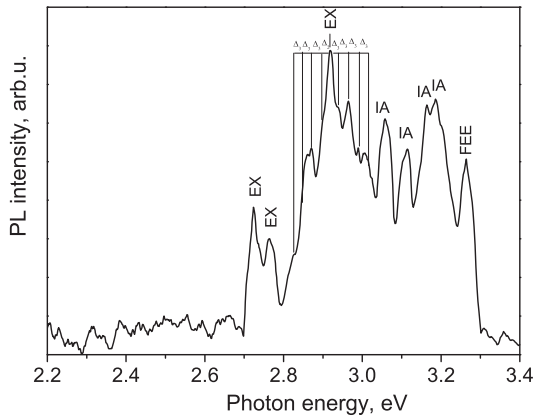


Fig. 4. PL spectra of anatase sample

when the power of a diode-pumped Nd:YAG laser was increased up to 70 mW and more. Amtout and Leonelli [10] used a tunable dye laser (pumped by a pulsed XeCl laser) with the intensity per pulse of about $2.5 \times 10^6 \text{ W}\cdot\text{cm}^{-2}$ to excite the PL in rutile single crystals. They observed a well-resolved PL structure with six peaks at low temperatures (12–200 K). In our case, the pulse intensity of an N_2 -laser is significantly higher (up to $4.4 \times 10^{10} \text{ W}\cdot\text{cm}^{-2}$), so we are able to register the PL peak at 2.91 eV along with other peaks forming a well-resolved band structure. To our knowledge, such a fine structure was not observed earlier in the PL spectra of TiO_2 at low or room temperatures.

The PL peak positions observed for *R* and *A* TiO_2 samples in Figs. 3 and 4 are similar, but the relative intensities of these peaks are different. We assume that the differences in the emission intensity from the *R* and *A* TiO_2 are connected with the different nature of excitons involved in the PL. Note that the high-power laser irradiation could promote phase transformation from anatase to rutile, as recently observed in TiO_2 powders [30, 31]. However, it was shown that, in air or oxygen atmosphere, the laser irradiation was unable to activate any phase transition in TiO_2 . Anatase keeps stable under the cw Nd:YAG laser irradiation with energy up to $10^6 \text{ J}/\text{cm}^2$, well above the threshold required to induce the anatase-to-rutile phase transition without oxygen or at low pressure. In our study, the energy load on the TiO_2 sample was about $300 \text{ J}/\text{cm}^2$, i.e. by more than 1000 times less than in the above-mentioned works. Thus, the possibility of the anatase-to-rutile transformation

can be neglected. To our knowledge, no overheating or degradation of the samples was observed in experiments with other semiconductor oxides [32], when used a similar pulsed N_2 laser technique as in our work, due to the N_2 laser short pulse duration and the low repetition rate.

3.4.1. Excitonic PL

Considering the PL spectra in Figs. 3 and 4, one can see that, as compared with *A* TiO_2 (Fig. 4), the PL of *R* TiO_2 (Fig. 3) shows a marked increase of the emission in the range 2.3–2.6 eV. This emission was observed also in other works, and it is usually attributed to PL from TiO_2 surface states [33]. Some PL peaks in the region 2.7–3.0 eV can be attributed to the $e^- - h^+$ recombination of photoinduced electrons and holes. The energies of two sharp peaks at 2.71 and 2.75 eV are very close to the trap energy levels located at 0.41–0.64 eV [12] below the CB, which were attributed to the oxygen vacancies with two trapped electrons (*F*-center) [28, 34]. The oxygen vacancies are a kind of intrinsic defects in the TiO_2 lattice forming intermediate energy levels within the TiO_2 band gap [35], which act as recombination centers for photoinduced electrons and holes. Therefore, this emission can arise from the $e^- - h^+$ recombination via oxygen vacancies. The strong excitonic PL peak at 2.91 eV can be reasonably attributed to the recombination of STE or free excitons, as frequently observed in different TiO_2 structures: single crystals [7, 9], nanoparticles [13], and colloidal nanoparticles [12, 29].

As is seen in Figs. 3 and 4, the PL excitonic peaks (EX) in *R* and *A* TiO_2 powder show a well-resolved fine structure. The differences in energy between the adjacent peaks in *R* TiO_2 PL are approximately equal to the values $\Delta = 22 \text{ meV}$ (183 cm^{-1}) or $\Delta_1 = 48 \text{ meV}$ (387 cm^{-1}). These values correspond to $\nu_1 = 183 \text{ cm}^{-1}$ ($\text{TO } E_u$) and $\nu_2 = 388 \text{ cm}^{-1}$ ($\text{TO } E_u$) phonons in the IR spectra of TiO_2 single crystals [15]. The differences in energy between the adjacent peaks in *A* TiO_2 PL spectra are close to the values of $\Delta_2 = 17 \text{ meV}$ (142 cm^{-1}) and $\Delta_3 = 24 \text{ meV}$ (193 cm^{-1}) that correspond to Raman-active optical phonon modes $\nu_3 = 146 \text{ cm}^{-1}$ (E_g) and $\nu_4 = 194 \text{ cm}^{-1}$ (E_g) (Fig. 1, Table 2).

Table 3 summarizes the observed excitonic PL emission peaks and their assignment to *R* and *A* TiO_2

Table 3. Raman active optical phonon modes of rutile and anatase TiO₂ samples

Rutile			Anatase		
$h\nu$, eV	$h\nu_{\text{ex}} - h\nu$, meV	Assignment	$h\nu$, eV	$h\nu_{\text{ex}} - h\nu$, meV	Assignment
2.998	-87	EX + 4 ν_1	3.015	-97	EX + 4 ν_4
2.981	-70	EX + 3 ν_1	2.991	-73	EX + 3 ν_4
2.953	-42	EX + 2 ν_1	2.964	-46	EX + 2 ν_4
2.931	-20	EX + ν_1	2.940	-22	EX + ν_4
2.911	-	EX	2.918	-	EX
2.868	43	EX - ν_2	2.900	18	EX - 4 ν_3
2.840	66	EX - $\nu_2 - \nu_1$	2.871	47	EX - $\nu_3 - \nu_4$
2.819	92	EX - $\nu_2 - 2\nu_1$	2.852	66	EX - $\nu_3 - 2\nu_4$
2.806	-	EX1	2.823	95	EX - $\nu_3 - 3\nu_4$
2.756	-	EX2	2.764	-	EX1
2.736	20	EX2 - ν_1	2.721	-	EX2
2.713	-	EX3			
2.665	48	EX3 - ν_2			
2.640	73	EX3 - $\nu_2 - \nu_1$			
2.621	92	EX3 - $\nu_2 - 2\nu_1$			

optical phonon modes. Thus, the EX peaks and their phonon replicas arise as a result of the strong exciton-phonon interaction in the TiO₂ structure under the high-power N₂-laser excitation. It is worth mentioning that our results correspond well with the results of [9, 10], where the exciton-phonon interaction was observed for *R* TiO₂ single crystal at low temperatures. The peaks at 2.957 and 2.902 eV [8], as well as 2.989, 2.977, 2.934, 2.839, and 2.737 eV [10], were attributed to the phonon replicas of free excitons.

3.4.2. Band-to-band PL

The PL of the studied TiO₂ samples in the high-energy part of the spectra at $h\nu > 3.0$ eV (Figs. 3 and 4) can be ascribed to the band-to-band electron transitions from CB to VB with assistance of the absorption or emission of phonons. According to Daude *et al.* [21] and comparing with the optical absorption spectra (Fig. 2), the PL peak at 3.05 eV can be ascribed to IA transitions $\Gamma_{1b} \rightarrow X_{2b}$. The PL peaks at 3.10 and 3.17–3.19 eV correspond to the indirect transition $X_{1b} \rightarrow \Gamma_3$. Thus, the same electronic transitions are involved in the optical absorption and photoluminescence processes. Some differences in the PL of *R* and *A* TiO₂ due to different band structures can be noticed in the range 3.20–3.30 eV. The peak at 3.24 eV in the PL spectra of rutile (Fig. 3) can be ascribed to the onset of the DA transition $X_1 \rightarrow X_1$

[19]. The PL peak at 3.26 eV in anatase (Fig. 4) corresponds to a band gap of 3.29 eV for *A* TiO₂ [36] and can be ascribed to the free exciton emission (FEE) near the band edge. Notice that the PL peak at 3.03 eV in rutile (Fig. 3) is not clearly seen in PL measurements, and it has never been observed in *R* TiO₂ at room temperature before. However, this peak was observed in *R* TiO₂ at low temperatures [9] and was ascribed to FEE.

The anti-Stokes emission within 3.01–3.3 eV observed in *R* TiO₂ under the N₂ laser irradiation ($h\nu = 3.68$ eV) shows that excited electrons at the top level of the CB can be transferred not only to the bottom of the CB, but also on the relatively stable levels located higher than the CB bottom. We believe that the nature of the anti-Stokes PL emission in TiO₂ is rather complicated and requires further researches. However, in general, the results of this study correlate with our previous research of TiO₂ nanocrystalline powders [36–37].

4. Conclusions

We studied the laser-excited room-temperature PL of nanocrystalline anatase and rutile TiO₂ powders prepared by the thermal hydrolysis method. Using a high-intensity N₂ laser excitation, we observed the well-resolved peaks of PL emission of excitonic and band-to-band transitions in both *A* and *R* TiO₂ samples.

The sharp PL peaks at 2.71–2.81 eV arise from the excitonic $e^- - h^+$ recombination via oxygen vacancies in the TiO₂ structure. The strong excitonic PL peak at 2.91 eV is attributed to the recombination of self-trapped excitons in anatase or free excitons in rutile. The TO E_u (22 meV) and TO E_u (48 meV) phonons in rutile and E_g (17 meV) and E_g (24 meV) optical phonons in anatase and their replicas are observed as a result of the strong exciton-phonon interaction under the intense UV laser excitation.

The PL peaks within 3.03–3.26 eV in *A* and *R* TiO₂ are ascribed to indirect and direct phototransitions, which arise from the band-to-band $e^- - h^+$ recombination. The PL peaks, located at 3.03 eV in rutile TiO₂ and at 3.26 eV in anatase, can be attributed to the free exciton band edge emission.

The work was supported by the National Academy of Sciences of Ukraine under the Research Program “Nanophysics and Nanoelectronics” (Project No. VC-157).

1. X. Chen and S.S. Mao, Chem. Rev. **107**, 2891 (2007).
2. A. Fujishima, X. Zhang, and D.A. Tryk, Surf. Sci. Rep. **63**, 515 (2008).
3. U. Diebold, Surf. Sci. Rep. **48**, 53 (2003).
4. M. Anpo and Y. Kubokawa, Rev. Chem. Intermed. **8**, 105 (1987).
5. D.K. Pallotti, E. Orabona, S. Amoroso, C. Aruta, R. Bruzzese, F. Chiarella, S. Tuzi, P. Maddalena, and S. Lettieri, J. Appl. Phys. **114**, 043503 (2013).
6. L. Chiodo, J.M. García-Lastra, A. Iacomino, S. Ossicini, J. Zhao, H. Petek, and A. Rubio, Phys. Rev. B **82**, 045207 (2010).
7. H. Tang, H. Berger, P.E. Schmid, and F. Levy, Solid State Commun. **87**, 847 (1993).
8. M. Watanabe, T. Hayashi, H. Yagasaki, and S. Sasaki, Int. J. Mod. Phys. B **15**, 3997 (2001).
9. L.G.J. De Haart and G. Blasse, J. Solid State Chem. **61**, 135 (1986).
10. A. Amtout and R. Leonelli, Phys. Rev. B **51**, 6842 (1995).
11. V. Melnyk, V. Shymanovska, G. Puchkovska, T. Bezrodna, and G. Klishevich, J. Mol. Struct. **744-747**, 573 (2005).
12. N. Serpone, D. Lawless, and R. Khairutdinov, J. Phys. Chem. **99**, 16646 (1995).
13. L.V. Saraf, S.I. Patil, S.B. Ogale, S.R. Sainkar, and S.T. Kshirsager, Int. J. Mod. Phys. B **12**, 2635 (1998).
14. V.V. Shymanovskaya, A.A. Dvernyakova, and V.V. Strelko, Izv. AN SSSR, Neorg. Mater. **24**, 1188 (1988).
15. S.P.S. Porto, P.A. Fleury, and T.C. Damen, Phys. Rev. **154**, 522 (1967).
16. M. Gotic, M. Ivanda, S. Popovic, S. Music, A. Sekulic, A. Turkovic, and K. Furic, J. Raman Spectr. **28**, 555 (1997).
17. U. Balachandran and N.G. Error, J. Solid State Chem. **42**, 276 (1982).
18. J.C. Parker and R.W. Siegel, Appl. Phys. Lett. **57**, 943 (1990).
19. A.K. Ghosh, F.G. Wakim, and R.R. Addiss, jr., Phys. Rev. **184**, 979 (1969).
20. V.M. Khomenko, K. Langer, H. Rager, and A. Fett, Phys. Chem. Miner. **25**, 338 (1998).
21. N. Daude, C. Gout, and C. Jouanin, Phys. Rev. B **15**, 3229 (1977).
22. H. Tang, H. Berger, P.E. Schmid, and F. Levy, Solid State Commun. **92**, 267 (1994).
23. K. Vos and H.J. Krusemeyer, Solid State Commun. **15**, 949 (1975).
24. M. Anpo, N. Aikawa, Y. Kubokawa, M. Che, C. Louis, and E. Giamello, J. Phys. Chem. **89**, 5017 (1985).
25. Y. Zhu, C. Ding, G. Ma, and Z. Du, J. Solid State Chem. **139**, 124 (1998).
26. F. Dong, W. Zhao, Z. Wu, and S. Guo, J. Hazard. Mater. **162**, 763 (2009).
27. T. Sekiya, M. Igarashi, S. Kurita, S. Takekawa, and M. Fujisawa, J. Electron. Spectrosc. Relat. Phenom. **92**, 247 (1998).
28. K.V. Baiju, A. Zachariah, S. Shukla, S. Biju, M.L.P. Reddy, and K.G.K. Warriar, Catal. Lett. **130**, 130 (2009).
29. N.D. Abazovic, M.I. Comor, M.D. Dramicanin, D.J. Jovanovic, S.P. Ahrenkiel, and J.M. Nedeljkovic, J. Phys. Chem. B **110**, 25366 (2006).
30. H-Y. Lee, W-L. Lan, T.Y. Tseng, D. Hsu, Y-M. Chang, and J.G. Lin, Nanotechnology **20**, 315702 (2009).
31. P.C. Ricci, C.M. Carbonaro, L. Stagi, M. Salis, A. Casu, S. Enzo, and F. Delogu, J. Phys. Chem. C **117**, 7850 (2013).
32. A.N. Gruzintsev and W.T. Volkov, Semiconduct. **45**, 1420 (2011).
33. N.M. Rahman, K.M. Krishna, T. Soga, T. Jimbo, and M. Umeno, J. Phys. Chem. Solids **60**, 201 (1999).
34. Y. Lei, D. Zhang, G.W. Meng, G.H. Li, X.Y. Zhang, C.H. Liang, W. Chen, and S.X. Wang, Appl. Phys. Lett. **78**, 1125 (2001).
35. A. Janotti, J.B. Varley, P. Rinke, N. Umezawa, G. Kresse, and C.G. Van de Walle, Phys. Rev. B **81**, 085212 (2010).
36. L. Kernazhitsky, V. Shymanovska, T. Gavrliko, V. Naumov, V. Kshnyakin, and T. Khalyavka, J. Solid State Chem. **198**, 511 (2013).
37. L. Kernazhitsky, V. Shymanovska, T. Gavrliko, V. Naumov, and V. Kshnyakin, Ukr. J. Phys. Opt. **14**, 15 (2013).

Received 1.10.2013

*Л. Кернажицькій, В. Шимановська, Т. Гаврилко,
В. Наумов, Л. Федоренко, В. Кишнякін, Я. Баран*

ЗБУДЖЕНА ЛАЗЕРОМ
ЕКСИТОННА ЛЮМІНЕСЦЕНЦІЯ
НАНОКРИСТАЛІЧНИХ ПОРОШКІВ TiO₂

Резюме

Оптичне поглинання і фотолюмінесценція діоксиду титану TiO₂ вивчалися при кімнатній температурі. Нанокристалічні порошки TiO₂ були синтезовані зі структурою чистого анатазу або рутилу. Зразки було досліджено методами рентгенівської дифракції, рентгенівської флуоресценції, спектроскопії комбінаційного розсіювання світла, оптичного поглинання і фотолюмінесценції (ФЛ). Спектри ФЛ досліджувалися при інтенсивному УФ (3,68 еВ) збудженні N₂

лазером. Деякі цікаві особливості в спектрах ФЛ, в тому числі піки екситонних і міжзонних переходів в TiO₂ з високим спектральним розділенням, спостерігалися, за нашими даними, вперше. Показано, що смуги ФЛ, в тому числі піки при 2,71–2,81 еВ, і їх фонні повторення в спектрах анатазу і рутилу TiO₂ виникають внаслідок екситонної $e^- - h^+$ рекомбінації поблизу кисневих вакансій. Екситонний пік при 2,91 еВ віднесено до рекомбінації автолокалізованих екситонів в анатазі або вільних екситонів в рутилі TiO₂. Піки ФЛ у межах 3,0–3,3 еВ в анатазі TiO₂ приписано до непрямих дозволених переходів внаслідок зона-зона $e^- - h^+$ рекомбінації. Піки при 3,03 еВ і 3,26 еВ віднесено до емісії вільних екситонів поблизу фундаментального краю поглинання рутилу і анатазу TiO₂ відповідно. Обговорено вплив кристалічної структури TiO₂ на спектри ФЛ.